Politecnico di Torino

POLITECNICO Di TORINO

Environmental and Land Engineering

Master's Degree Thesis

On the Turbulence Properties of Channel Flows with Suction

Supervisors:

Prof. Costantino Manes

Candidate:

Hamidreza Torang

October 2024

Acknowledgments

I am deeply indebted to my parents for their unwavering love, support, and encouragement throughout my academic journey. Their belief in me has been a constant source of motivation and strength.

I would like to express my sincere gratitude to **Professor Costantino Manes**, my supervisor, for his invaluable guidance and mentorship. His expertise and patience have been instrumental in my academic growth.

I am also grateful to Roberto Bosio and Andrea Cagninei for their technical expertise and assistance.

Finally, I would like to acknowledge the faculty of the Department of Environmental and Land Engineering for their academic guidance and the stimulating learning environment they have provided. Their dedication to their field has inspired me to pursue my research interests.

Abstract

This experimental study investigates the effects of membrane-induced suction on turbulent flow characteristics within a rectangular channel at a Reynolds number of 1000. Benchmark tests without the membrane confirmed the turbulent nature of the flow at this Reynolds number, making it a suitable choice for the study. Suction was generated by adjusting the bulk pressure within the test section and modifying pump frequency. Laser Doppler anemometry (LDA) was employed to measure velocity fluctuations, enabling the quantification of turbulence intensity and power spectral density. Results demonstrate a significant reduction in both turbulence intensity and velocity variance under various suction conditions compared to the benchmark case. Surprisingly, the turbulent intensity was found to be independent of the suction rate.

The analysis reveals that suction effectively dampens turbulent eddies, particularly near the membrane surface. The study further explores the relationship between suction rate and turbulent flow properties.

Suction contributes to the enlargement of near-wall streak length by damping turbulent fluctuations and stabilizing the flow near the wall. The near-wall streaks length at point B (located at 2.5 mm from the bottom of channel) is greater than at point A (located at the center of channel) in both benchmark and suction cases that is indicative of the higher shear stress and elongated turbulent structures in this region.

The findings of this research have important implications for the design and optimization of membrane-based processes. By understanding the effects of suction on turbulence in rectangular channels, it is possible to improve membrane performance, reduce fouling, and enhance overall system efficiency. Future studies should concentrate on exploring the influence of membrane types, varying Reynolds numbers on turbulent flow dynamics in the presence of suction.

Keywords: Turbulence, Suction, Membrane, Water Treatment, LDA, Turbulence Intensity, Spectral Analysis.

Contents

List of Figures

List of Tables

List of Acronyms

DNS	Direct Numerical Simulation
LES	Large Eddy Simulation
Γ	Suction Rate
V	Transpiration Velocity
U_∞	Free-Stream Velocity
TASBL	Turbulent Asymptotic Suction Boundary Layer
DN25,32,250	Pipe Nominal Diameter 25 mm, 32 mm, and 250 mm
AR	Aspect Ratio
Re	Reynolds Number
U	Mean Bulk Velocity
h	Semi-Height of Channel
ν	Kinematic Viscosity of Water
LDA	Laser Doppler Anemometry
BSA	Burst Spectrum Analyzer
P	Instantaneous Pressure
PES	Polyether Sulfone
MWCO	Molecular Weight Cut-Off
Da	Dalton
T	Temperature
V_m	Mean Vertical Velocity
Q	Flow Rate
A	Cross-Sectional Area of the Membrane
PIV	Particle Image Velocimetry
U_m	Mean Longitudinal Velocity
I_T	Turbulent Intensity
PSD	Power Spectral Density
SD	Standard Deviation
U_{max}	Maximum Mean Velocity
u^*	Friction velocity
f	Frequency
λ	Average near-wall Streak Length
λ^+	Normalized near-wall Streak Length

Chapter 1

Introduction

The escalating global population has significantly increased the demand for freshwater. According to the United Nations World Water Development Report, global water demand has been rising by approximately 1% annually since the 1980s, driven by factors such as population growth, economic development, and shifting consumption patterns [1]. Climate change further complicates water management by linking water demand to weather variables. For instance, water demand can surge by 9-10% during the hottest weeks, with variations depending on the social characteristics of the users [2].

Given these challenges, efficient water resource management is paramount. Various water treatment technologies, including membrane-based systems, biological treatments, and electrochemical treatments, have been developed to address these issues. Among these, membrane technologies such as reverse osmosis, nanofiltration, ultrafiltration, and microfiltration are particularly noteworthy for their high contaminant removal efficiencies, compact design, and potential for resource recovery. However, these systems face substantial challenges related to fouling, concentration polarization, and operational efficiency [3].

To mitigate membrane fouling, different hydrodynamic methods, such as pulsating, vibrating, rotating, and helicoidal flows, have been explored. Studies have demonstrated that these methods can influence the behavior of turbulent wall flows, which is crucial for reducing fouling and enhancing membrane performance [4-5].

Investigating turbulent wall flows, especially in the presence of suction induced by membranes, is essential for understanding how such conditions affect turbulence properties. The study of turbulence properties in channel flows with suction has garnered significant attention due to its potential applications in fluid dynamics and engineering. Suction, as a method of boundary layer

control, has been shown to influence various aspects of turbulent flow, including velocity fluctuations, boundary layer development, and turbulence intensity.

While most studies on turbulent wall flows with suction have been conducted in aerodynamic contexts, such as the development of turbulent boundary layers in wind tunnels, there has been limited research on the hydrodynamic aspects, particularly in channel flows [6-11]. Some studies in aerodynamics have used numerical simulations, including direct numerical simulations (DNS) and large eddy simulations (LES), to examine the effects of uniform suction over flat plates [12]. However, hydrodynamic experimental investigations, which are crucial for validating these simulations and providing practical insights, remain underexplored [4].

This thesis aims to investigate the effects of membrane-induced suction on turbulence in channel flows, which is vital for mitigating membrane clogging and concentration polarization. Specifically, the research questions guiding this thesis are as follows:

1. How does turbulence intensity change with different suction rates at the same Reynolds number?
2. How is the velocity variance of turbulent eddies distributed across different frequency bands under varying suction conditions?

By answering these questions, this research will contribute to a deeper understanding of the interplay between suction and turbulence in channel flows, offering potential solutions to improve the efficiency of membrane-based water treatment systems.

Chapter 2

Literature review

The suction intensity in most studies is quantified using the suction rate parameter (Γ), defined as the ratio of transpiration velocity (V) to free stream velocity (U_∞). The transpiration velocity represents the rate at which fluid is injected or removed from a porous surface, while the free stream velocity is the fluid velocity far from the surface where boundary layer effects are minimal. When the suction rate exceeds $3\text{-}4\times10^{-3}$, turbulence is eliminated, leading to relaminarization. Conversely, if the suction rate falls below this threshold, turbulence persists [13].

Ferro demonstrated that in a turbulent asymptotic boundary layer, the mean velocity profile effectively scales with outer coordinates, regardless of the suction rate [6]. Conversely, Bobke suggested that the classical logarithmic law of the wall is more suitable for inner scaling [14].

Regarding other velocity statistics, the literature consistently shows that suction significantly reduces both normal and shear Reynolds stresses throughout the entire boundary layer. Several studies also offer insights into the behavior of Reynolds stresses under suction. Schildknecht's research indicated a reduction in the amplitudes of velocity fluctuation components, which are directly related to normal Reynolds stresses [15]. Antonia et al. provided detailed measurements of local wall shear stress and Reynolds stresses downstream of a concentrated suction strip, revealing that Reynolds shear stress recovers slowly after pseudo-relaminarization [16]. Although Yoshioka's study did not explicitly focus on Reynolds stresses, its findings on turbulence intensity suppression offer indirect insights into the behavior of these stresses in the boundary layer [7]. Tennekes' application of similarity laws provides a theoretical basis for inferring Reynolds stress behavior in turbulent flows with suction, adding another layer of understanding to this complex phenomenon [8].

Marco Ferro, Shuya Yoshioka, T. J. Black, and A. J. Sarnecki have shown that suction can effectively manipulate the boundary layer by delaying the transition from laminar to turbulent flow

and preventing flow separation [6,7,9]. Ferro's research explored the development of a Turbulent Asymptotic Suction Boundary Layer (TASBL), demonstrating that the mean velocity profile remains constant along the streamwise direction when controlled exclusively by the suction rate [6].

Studies by Shuya Yoshioka and T. J. Black & A. J. Sarnecki have shown that suction effectively suppresses turbulence intensity, especially in the outer regions of the boundary layer. This suppression creates a more stable flow regime, which is essential for applications demanding precise control of boundary layer characteristics. The reduction in turbulence intensity, combined with the ability to delay the transition from laminar to turbulent flow, highlights the efficacy of suction as a boundary layer control mechanism [7,9].

The application of similarity laws, such as the "law of the wall" and the "velocity defect law" has also been a focus in understanding turbulent boundary layers with suction. H. Tennekes and T. J. Black & A. J. Sarnecki applied these laws to describe the behavior of turbulent boundary layers under suction, providing a robust theoretical framework that can predict the effects of suction on flow dynamics [8-9].

Another significant finding in the literature pertains to the attainment of asymptotic states in turbulent boundary layers. Both Alexandra Bobke and Marco Ferro's studies highlight that an asymptotic turbulent boundary layer (TASBL) can be achieved when the mean velocity profile remains constant along the streamwise direction, controlled exclusively by the suction rate [6,14].

The diversity in experimental setups across these studies, however, introduces some variability in the results. While some studies utilized wind tunnels, such as those by J. M. Kay and R. A. Dutton, others, like T. Khapko and Yukinori Kametani, employed direct numerical simulations (DNS) [10,11,12,17]. These differences in methodology can lead to variations in observed phenomena, such as the specific impacts on friction drag. For instance, Kametani's study uniquely addressed the effects of both suction and blowing on friction drag, finding that while uniform blowing reduces skin friction, uniform suction increases it. This finding is not widely discussed in another research [17].

Suction, whether concentrated or distributed, can significantly impact the behavior of boundary layers. R. A. Antonia's research focused on concentrated wall suction, demonstrating that it can

cause pseudo-relaminarization almost immediately downstream of a suction strip [16]. In contrast, R. A. Dutton's study on distributed suction highlighted how it can maintain boundary layer thickness over a broad surface area and even revert to laminar flow at sufficiently high suction rates [10].

T. Khapko and his colleagues conducted an intriguing study on turbulence collapse in asymptotic suction boundary layers (ASBL). Their research revealed that turbulence can collapse when the Reynolds number decreases below a critical threshold, leading to the formation of transient, elongated structures aligned with the flow direction. This phenomenon, not observed in previous studies, represents a significant contribution to the field [12].

Despite significant progress in understanding the influence of suction on channel flow turbulence, a notable gap remains in scientific literature. Most studies have been limited to specific conditions and narrow suction rates, underscoring the need for a more comprehensive investigation at constant Reynolds numbers across a broader range of suction rates. By exploring how varying suction rates at a given Reynolds number, affect turbulence characteristics, we can potentially unlock valuable insights for engineering and fluid dynamics applications. Addressing this knowledge gap is essential for advancing the field and maximizing the practical utility of suction in real-world scenarios.

This study aims to enhance previous research by conducting innovative experiments that investigate suction at a low Reynolds number of 1000 across various suction rates. Unlike previous studies, this research maintains a low Reynolds number, slightly above the transitional phase commonly observed in membrane technology. Membrane systems operate in crossflow conditions, analogous to suction wall flows where permeation is the vertical mass flux associated with suction. This permeating flux is driven by pressure differences between the fluid in the feed and the surrounding area. To optimize mixing and minimize membrane clogging, the feed flow in these systems is kept turbulent.

Understanding turbulence behavior under suction is essential for mitigating membrane clogging, as it primarily drives mass transfer at the membrane-feed interface. In the realm of fluid mechanics, the effects of permeating flux (suction) on turbulence have been relatively unexplored. This study aims to bridge this knowledge gap.

Chapter 3

Experimental Methods

3.1 Overall description of the facility

This chapter provides a detailed overview of the experimental facility utilized for conducting all the experiments presented in the study. (see figure 1)

Two distinct types of experiments were carried out. The first experiment, commonly referred to as the benchmark test, involved a channel flow system with smooth, impermeable boundaries constructed from Perspex material (see figure 2). This setup served as a baseline for comparison.

In contrast, the second experiment, referred to as the filtration test, modified the experimental setup by replacing the impermeable bottom wall with a thin membrane placed on top of a highly permeable porous medium made of metallic foam. This porous material was positioned over a Plexiglass base that was divided into three separate compartments. These compartments played a crucial role in collecting the filtered water and ensuring that the filtration rates remained spatially uniform throughout the experiments (see figures 3, 4).

The benchmark test was crucial for establishing a standard reference point to evaluate and compare the flow behavior over a porous membrane in the filtration test. The images that follow illustrate the two different hydraulic plant configurations used during the experiments (see figures 2,3). These setups allowed for a systematic investigation of the differences between impermeable and porous boundary conditions under controlled experimental conditions.

Fig.1 Overall setup of the hydraulic plant .

Fig.2 Benchmark Case: Flow Without Filtration.

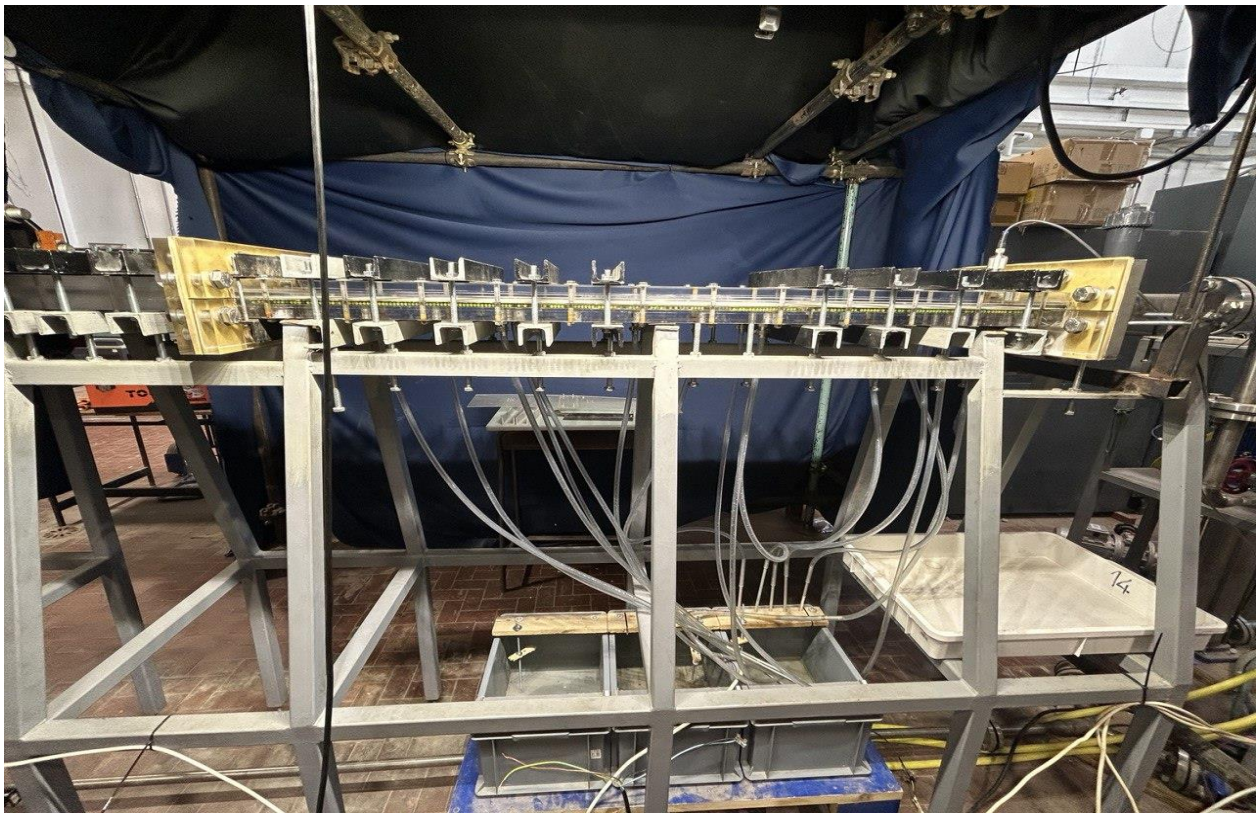

Fig.3 Filtration Case: Drainage and Buckets.

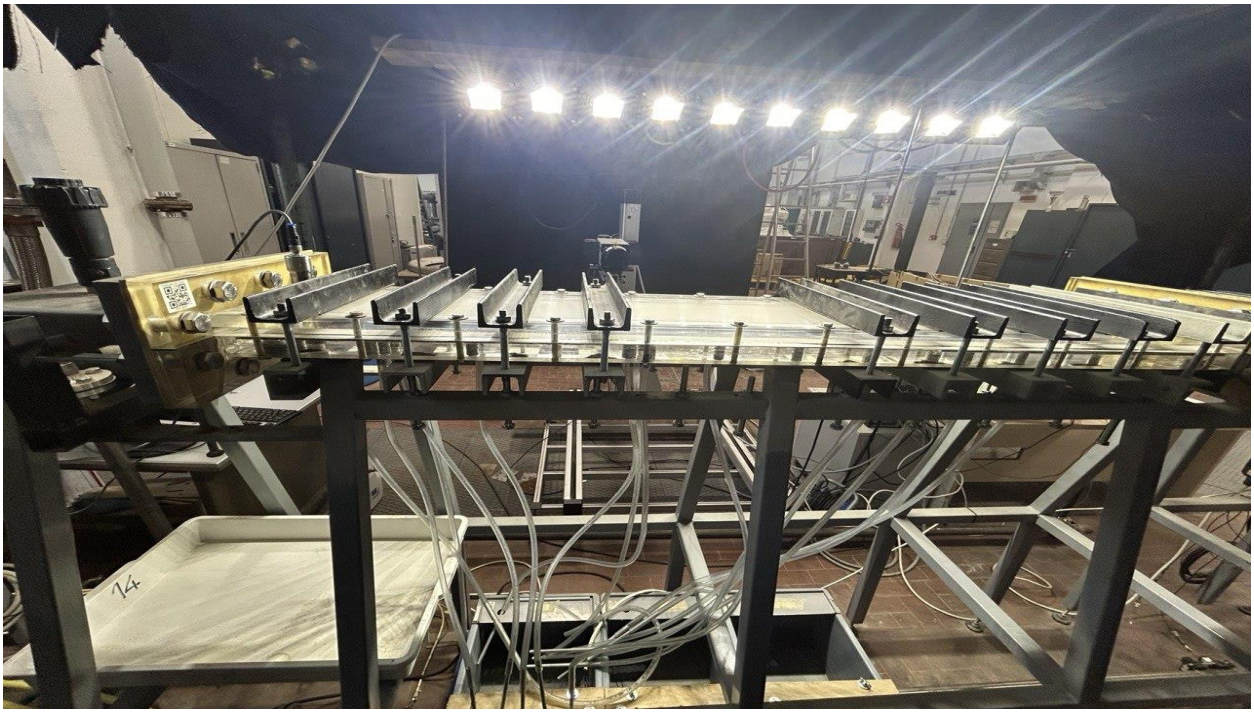

Fig.4 Filtration Case: Alternate view of Drainage and Buckets.

The experimental facility was designed to operate in a recirculating water circuit, utilizing a tap water supply. As illustrated in Figure 1, the facility comprises several interconnected components, which will be described in detail below.

A constant-head tank with a volume of 1 m^3 served as the water reservoir. A thermocouple was embedded within the tank to monitor the water temperature. To maintain a constant temperature during experiments, a 5-kW chiller was employed. The viscosity of water and membrane hydraulic conductivity are known to be temperature-dependent, making temperature control crucial.

Two parallel multistage pumps, each with a different power rating, were utilized to circulate water within the facility. These pumps, capable of achieving a maximum total flow rate of 2.4 l/s, were installed in separate pipe branches. Ball valves positioned in line with the pumps allowed for selective flow direction from the tank to the rest of the system. By individually operating each pump at varying power levels, it was possible to establish a range of flow regimes within the test section, transitioning from laminar to turbulent flow. This enabled the study of a broad spectrum of Reynolds numbers, encompassing values from 135 to 1800.

Three different pipe sizes, DN25, DN32, and DN250, were incorporated into the experimental setup. The vertical pipes connecting to the constant-head tank were DN32, while the main horizontal pipelines were DN25. After the divergent section, DN250 pipes were used. To prevent excessive pressure buildup and regulate the flow within the system, a bypass was included, allowing a portion of the water to be diverted directly back to the tank.

Globe valves were installed in both the main pipeline and the bypass to control the flow rate. An ultrasonic flow meter, model AT600, was integrated into the main pipeline to measure water flow rate and velocity. The collected data was transmitted to a computer and visualized using a LabVIEW program.

To mitigate sudden flow changes that could induce turbulence, a divergent section was incorporated into the system. The water then passed through a conditioning unit equipped with a stilling chamber to ensure a uniform flow profile. A contraction section followed, preventing boundary layer separation and facilitating the development of an undisturbed boundary layer.

The connection section linked the conditioning unit to the main test section, which will be discussed in detail in the subsequent section. Two self-closing air release valves were installed,

one on the stilling chamber and the other at the end of the test section, to remove any trapped air from the water.

To monitor hydraulic pressure in real-time, a pressure sensor was placed at the end of the test section and connected to a computer via a LabVIEW program. A backpressure valve was positioned after the test section to regulate hydraulic pressure during experiments by controlling its opening and closing. The pipes downstream of the backpressure valve were connected to the tank, completing the recirculation loop.

For filtration tests, three separate 15-liter buckets were positioned beneath the test section to collect the filtered water. Drainage tubes directed the filtered water from the test section into these buckets. Ultrasonic level sensors were installed within the buckets to activate bilge pumps automatically when the water level reached a predetermined height. The bilge pumps then emptied the buckets into the main tank via recirculation tubes.

By adjusting the pump frequency and backpressure valve settings, the desired water velocity and pressure within the test section were achieved. A computer program controlled the pump frequency, regulating the rotational speed of the pump shaft. For a more comprehensive understanding of the hydraulic plant components, interested readers are encouraged to consult the work of Bert [4].

3.1.1 Description of the test section

Building upon the previously discussed experiment types (benchmark and filtration), the primary distinction between them lies within the test section, which constitutes the heart of the system. Two key design considerations guided the development of this section:

i) **Aspect Ratio (AR)**: Informed by prior research on confined cylinder flow within a rectangular duct (Li et al., 2023), an aspect ratio (AR) of 20 (width of the channel divided by its height) was adopted. This ensures comparability with numerical simulations and minimizes the influence of lateral walls on the flow behavior [19].

ii) **Hydrodynamic Entrance Region**: The region downstream of the channel inlet where the velocity profile achieves a fully developed and unchanging state is known as the hydrodynamic entrance region. To facilitate the establishment of this fully developed, self-similar flow, the channel length was designed to be a specific multiple of the channel height (2h) [20].

Fulfilling these design requirements, the test section comprises a rectangular channel constructed from transparent plexiglass. The channel dimensions are 1.45 m in length, 0.2 m in width, and 0.01 m in height. The plexiglass material permits optical access for the laser instrumentation employed during measurements.

For the sake of clarity, the origin of the reference system used in this study is placed at the bottom right corner of the test section's entrance. The X, Y, and Z coordinates correspond to the streamwise, wall-normal, and spanwise directions, respectively.

Ultimately, the test section was designed to replicate the dynamic and kinematic properties observed in industrial flows. To achieve this, three dimensionless numbers were employed:

i) **Suction Intensity (Γ):** Defined as the ratio of vertical velocity at the feed-membrane interface (V) to the bulk mean velocity of the overlying channel flow (U).

ii) **Reynolds Number (Re):** Defined as $U*h/\nu$, where U is the bulk mean velocity, h represents the semi-height of the channel, and ν denotes the kinematic viscosity of water.

iii) **Turbulence Intensity (I_T):** Defined as ratio of standard deviation (SD) to the maximum mean velocity (U_{max}).

In conclusion, the designed test section and system offer the flexibility to investigate a wide spectrum of flow regimes – from laminar to transitional to turbulent – across a broad range of Reynolds numbers (135 to 1800). Additionally, a substantial range of suction rates (up to two orders of magnitude) can be implemented during filtration experiments.

Figures 2 and 3 depict the test section utilized in both experiment types.

3.2 Experimental procedure and measuring equipment

This section outlines the experimental procedures and equipment employed for conducting the experiments. It is divided into two parts. The first part focuses on the benchmark case involving an impermeable wall flow, while the second part addresses the filtration tests.

3.2.1 measuring equipment

Longitudinal velocity measurements were conducted using Laser Doppler Anemometry (LDA), a non-intrusive, high-resolution technique capable of capturing high-frequency point measurements and providing a comprehensive power spectral analysis of turbulent kinetic energy distribution. (see figure 5) LDA's exceptional accuracy is achieved without requiring initial calibration, making it an invaluable tool for fluid dynamics research.

The operating principle of LDA involves the intersection of two laser beams of equal frequency and high intensity at an angle, forming an ellipsoidal measurement volume. (see figures 6, 7) As suspended particles traverse this volume, they scatter laser light, which is detected by a photomultiplier. By analyzing the Doppler shift between the incident and scattered light, the velocity of the particle can be determined. To ensure accurate measurements, the plane of the laser beams must be precisely aligned with the direction of flow within the test section. Achieving accurate alignment of the LDA and test section is critical to the reliability of the measurements. For this purpose, precision instruments such as spirit levels and laser levels are employed to ensure horizontal and vertical alignment. Even slight deviations from proper alignment can introduce significant errors into the results, emphasizing the importance of meticulous attention to this aspect of the experimental setup [18]. A threshold-based approach was used to filter out outliers from LDA measurements. Outliers were defined as velocity fluctuations that were significantly different from the average, exceeding a threshold of three times the standard deviation.

The precise positioning of the Laser Doppler Anemometer (LDA) was achieved through the utilization of a sophisticated computer-controlled traversing system, the ISEL iMC-S8. (see figure 8) This advanced apparatus is capable of detecting minute displacements with a sensitivity of 6 micrometers in all three spatial dimensions. Moreover, the origin of the traversing system was

carefully established at the base of the test section to ensure accurate measurements. The subsequent analysis of the acquired signals was conducted using a Dantec Dynamic Burst Spectrum Analyzer, the BSA F600-2D model. In conjunction with this specialized hardware, the BSA flow software, version 6.5, was employed to facilitate the comprehensive analysis of the collected data.

Fig.5 LDA Instrument.

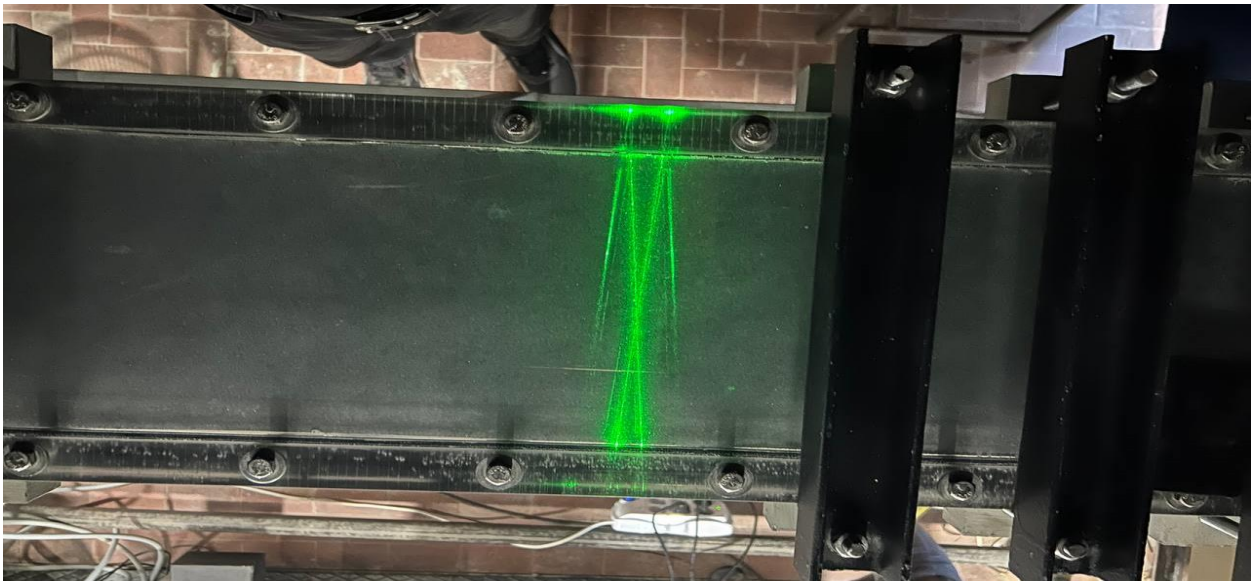
Fig.6 LDA Principle: Laser Beam Intersection.

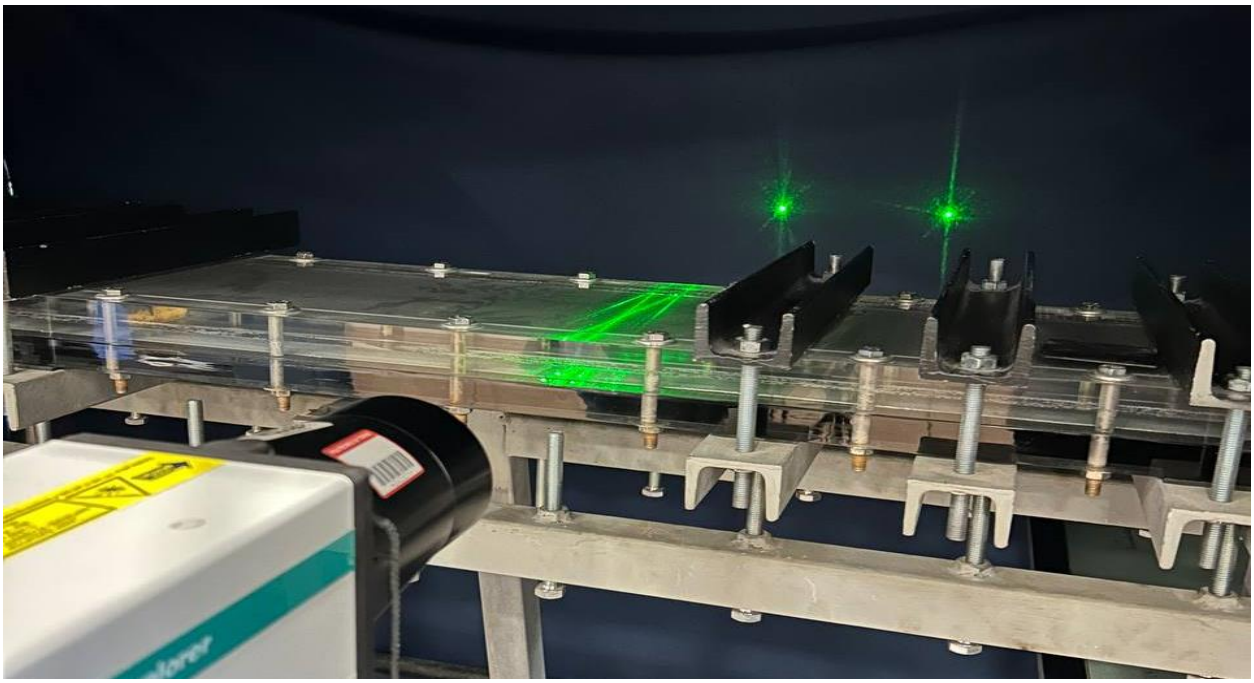

Fig.7 LDA Principle: Laser Beam Intersection (Alternate View).

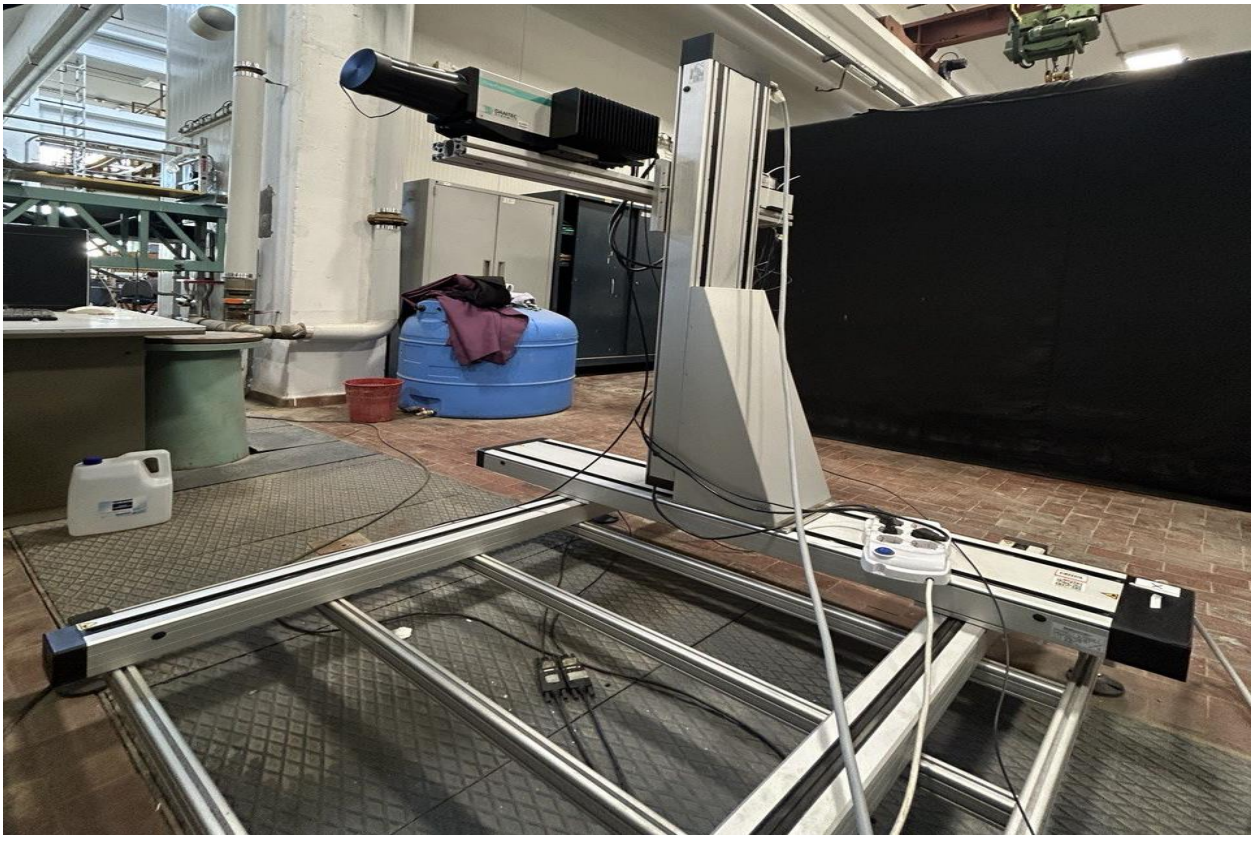

Fig. 8 Traverser for Probe Positioning of LDA.

3.2.2 Benchmark tests

The benchmark tests conducted in this study were performed at two specific locations within the test section:

i) **Point A**: Situated at the center of the test section, with coordinates X = 83.5 cm, Y = 0.5 cm, and Z = 10 cm.

ii) **Point B**: Located at X = 83.5 cm, Y = 0.25 cm, and Z = 10 cm.

At both points, the bulk mean velocity (U) was measured using a sensor. The mean longitudinal velocity and turbulent intensity were then calculated from the LDA measurements using MATLAB code.

Following the approach outlined by Ferro [6], the mean velocity profiles were scaled in outer coordinates using the maximum mean velocity (U_{max}). This method was adopted in the present study to facilitate the calculation of turbulence intensity (I_T).

A detailed summary of the experimental conditions is provided in Table 1. The table includes the Reynolds number (Re), instantaneous pressure measurements, and pump frequency settings. The Reynolds number was calculated using the formula Re = U*h/ν, where U is the mean bulk velocity, h is the semi-height of the channel and ν is the kinematic viscosity of water (approximately $10^{\wedge-6}$ m^2/s) and P is the instantaneous pressure that measured by pressure sensor.

Table.1 Summary of the experimental condition for benchmark case at both points. P is instantaneous pressure.

Test Name	Symbol	Coordinates [cm]	Re [-]	P [Bar]	U [m/s]
BN-A	*	x=83.5, y=0.5, z=10	1000	0.173	0.2
BN-B	*	x=83.5, y=0.25, z=10	1000	0.182	0.2

The benchmark tests were conducted by my colleague over a range of Reynolds numbers, starting from the lowest achievable value (Re = 135) and progressing to the maximum achievable Reynolds number (Re = 1800) within the hydraulic regime. These tests were performed within the test section with the aim of examining the transition of the flow from a laminar to a turbulent state. The results indicated that the flow remained in a laminar state up to approximately Re = 650. Between Re = 650 and Re = 1000, the flow exhibited transitional characteristics. Finally, at around Re = 1000 and beyond, the flow became self-sustained turbulent. This specific Reynolds number was subsequently utilized for the filtration tests. The velocity time series of the minimum Reynolds number (135) and filtration Reynolds number (1000) at points A and B are presented in the figures 9,10 and figures 11,12 respectively to illustrate the transition from laminar to turbulent flow.

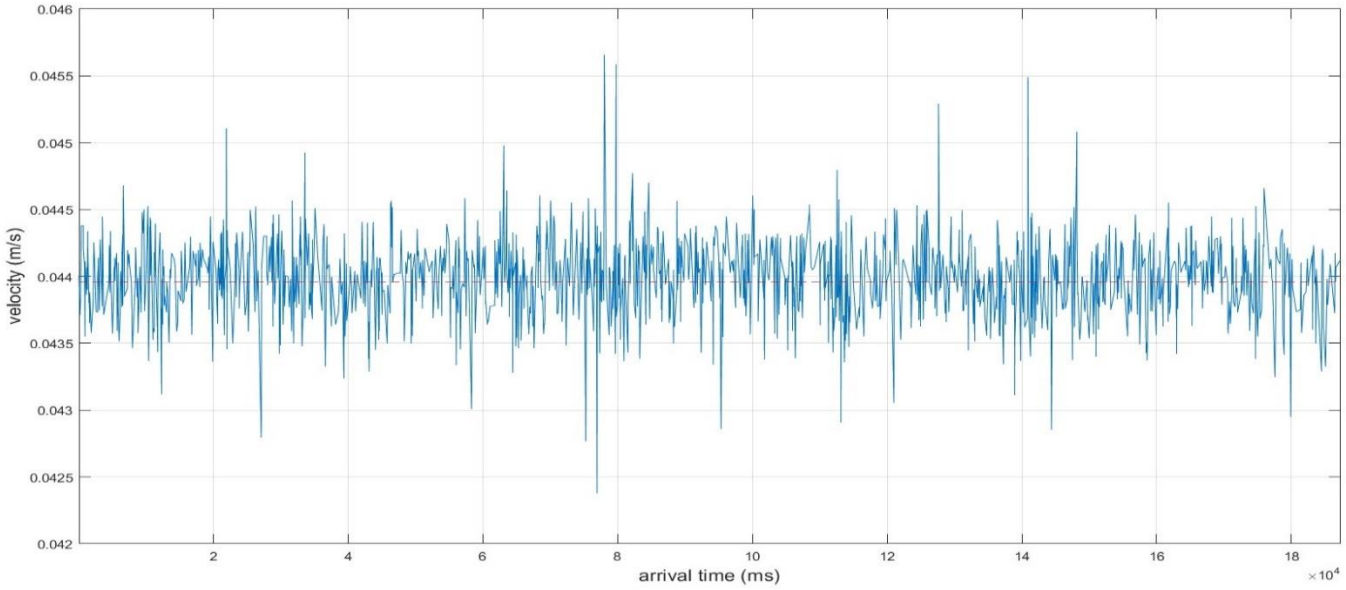

Fig.9 Velocity Time Series of Benchmark Case at Point A located at the center of channel (Re=135).

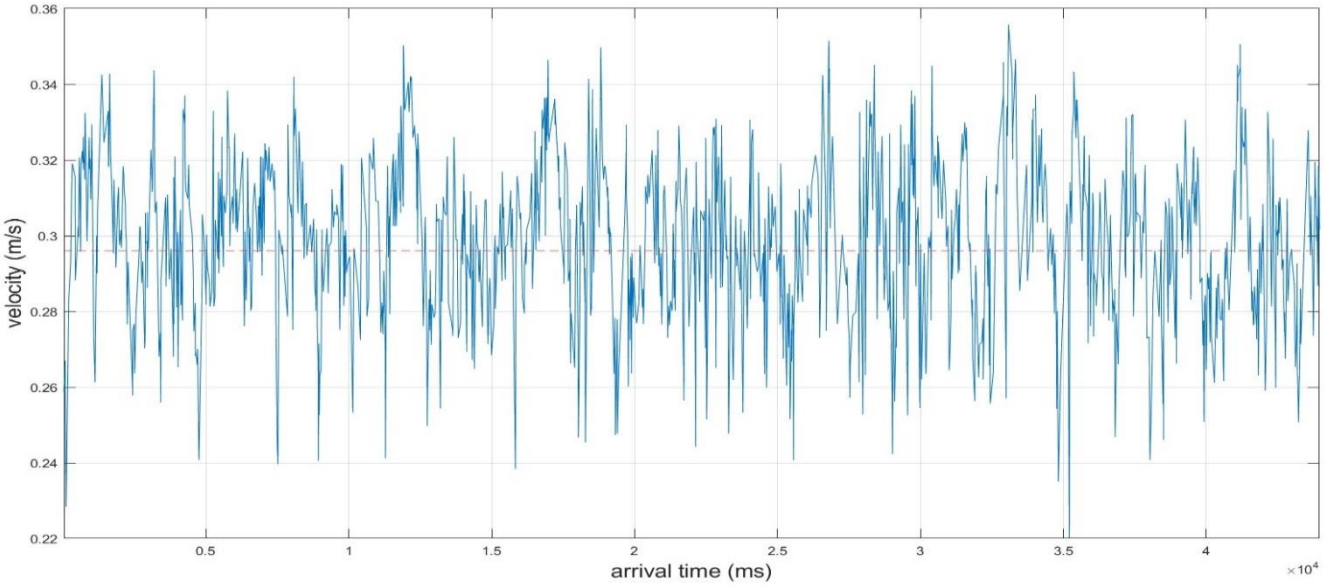

Fig.10 Velocity Time Series of Benchmark Case at Point A located at the center of the channel (Re=1000).

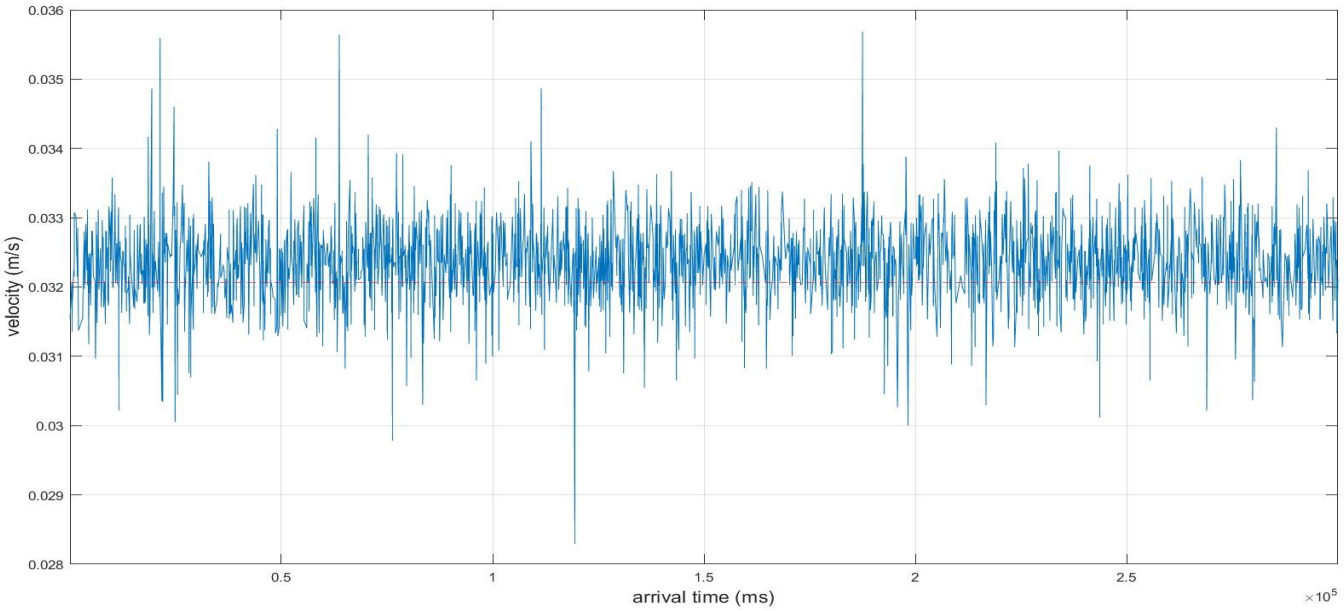

Fig.11 Velocity Time Series of Benchmark Case at Point B located 2.5 mm from the bottom of the channel (Re=135).

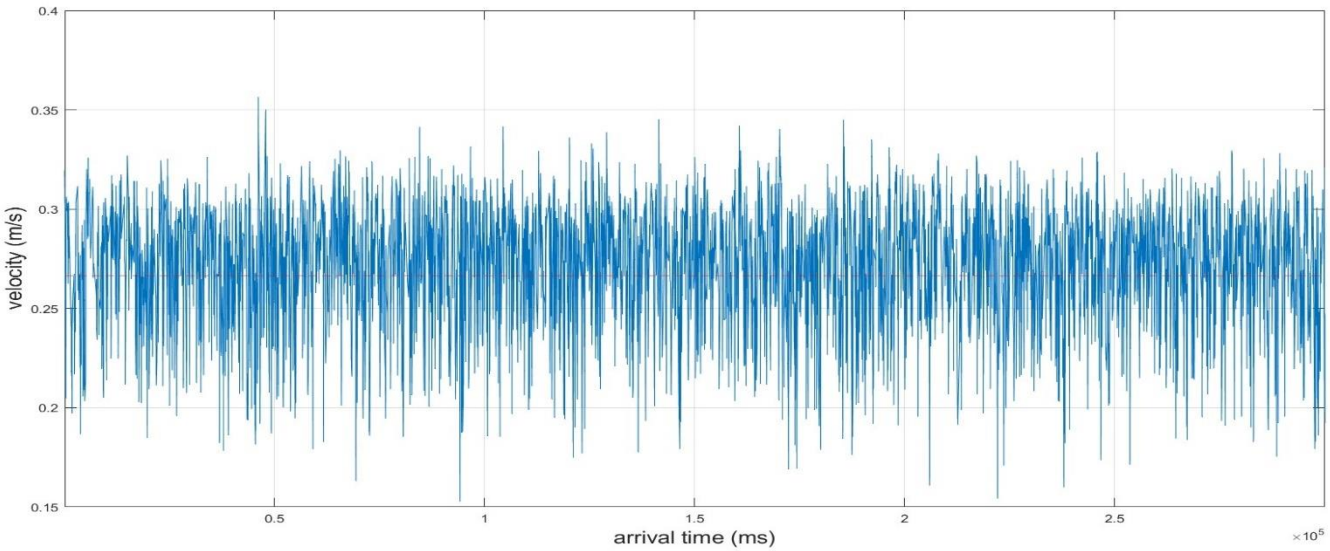

Fig.12Velocity Time Series of Benchmark Case at Point B located 2.5 mm from the bottom of the channel(Re=1000).

3.2.3 Filtration tests

The filtration tests deviated from the benchmark experiments in terms of the test section configuration. The impermeable lower section of the test section was replaced with a polyether sulfone (PES) Synder-LY ultrafiltration flat-sheet membrane (see figure 13). This membrane possessed a molecular weight cut-off (MWCO) of 100,000 Da and a nominal permeance ranging from 80 to 123 liters per square meter per hour per bar. The membrane was positioned atop a highly permeable porous medium composed of metallic foam (see figure 14). This assembly was mounted on a new lower section equipped with fifteen drainage tubes to facilitate the collection of filtered water into buckets placed beneath the test section (see figures 15).

Fig.13 Filtration Membrane.

Fig.14 Metallic Foam Support.

Fig.15 Drainage Tube System.

To mitigate the effects of temperature (T) on the kinematic viscosity and permeability of the membrane, efforts were made to maintain a consistent temperature within the range of 19 to 21 degrees Celsius. Furthermore, the applied pressure (p) was restricted to a maximum of 0.603 bar, which represented the safe operating pressure for the test section under suction. Exceeding this pressure could lead to system leakage, potentially compromising the accuracy of the results. Therefore, the specified pressure range ensured that the required conditions were met without compromising the integrity of the system.

Each filtration test was conducted over a period of approximately 45 minutes to allow for sufficient filtration. Once the water level in the buckets reached a critical point, a water level sensor measured the flux rate. The filtered water was then pumped out of the buckets using a bilge pump. By considering the volume of pumped water and the total filtration time, the mean vertical velocity of the membrane (V_m) was calculated using the continuity equation ($Q = A*V_m$), where Q is the flow rate and A is the cross-sectional area of the membrane.

The mean longitudinal velocity at both points was measured using an LDA instrument. It is important to note that the vertical velocity was assumed to be identical at points A and B due to the limitations imposed by the test section's height. While vertical velocity could not be measured using LDA, it could be determined using alternative techniques such as particle image velocimetry (PIV).

The hydraulic conditions for the filtration tests at points A and B are summarized in Tables 2 and 3, respectively.

Table.2 Summary of the experimental condition for filtration case at point A. P is instantaneous pressure.

Test Name	symbol	Coordinates [cm]	Re [-]	P [Bar]	U [m/s]
F-A-1	●	x=83.5, y=0.5, z=10	1000	0.105	0.205
F-A-2	■	x=83.5, y=05, z=10	1000	0.207	0.207
F-A-3	♦	x=83.5, y=0.5, z=10	1000	0.305	0.205
F-A-4	▲	x=83.5, y=0.5, z=10	1000	0.410	0.205
F-A-5	▼	x=83.5, y=0.5, z=10	1000	0.502	0.202
F-A-6	►	x=83.5, y=0.5, z=10	1000	0.603	0.203

Table.3 Summary of the experimental condition for filtration case at point B. P is instantaneous pressure.

Test Name	symbol	Coordinates [cm]	Re [-]	P [Bar]	U [m/s]
F-B-1	●	x=83.5, y=0.25, z=10	1000	0.105	0.205
F-B-2	■	x=83.5, y=0.25, z=10	1000	0.207	0.207
F-B-3	♦	x=83.5, y=0.25, z=10	1000	0.305	0.205
F-B-4	▲	x=83.5, y=0.25, z=10	1000	0.410	0.205
F-B-5	▼	x=83.5, y=0.25, z=10	1000	0.502	0.202
F-B-6	►	x=83.5, y=0.25, z=10	1000	0.603	0.203

For both Points A and B, the Reynolds number (Re) was calculated using the formula $Re = U*h/\nu$. The mean bulk velocity (U) in the test section was measured with a sensor, while the kinematic viscosity (ν) of the water was determined for a temperature range of 19 to 21°C. The mean longitudinal velocity was measured using Laser Doppler Anemometry (LDA).

Chapter 4

Results and discussion

The results section is divided into two primary subsections.

The first subsection focuses on the relationship between turbulence intensity and various suction rates at a constant Reynolds number. In this analysis, we explore how the level of turbulence is influenced by different suction intensities.

The second subsection delves into the frequency-based distribution of velocity variances. This analysis provides insights into the spectral composition of turbulence and the dominant frequency ranges contributing to the overall energy content.

4.1 Turbulence intensity vs. suction intensity

In this section, we present a detailed analysis of the measurement results obtained for both benchmark and filtration scenarios.

The mean longitudinal velocity was determined using Laser Doppler Anemometry (LDA) for both benchmark and filtration tests. To calculate the mean longitudinal velocity and turbulence intensity, specialized MATLAB codes were employed. The transpiration velocity was calculated as previously described for each test. Furthermore, the turbulence intensity (I_T) is ratio of standard deviation (SD) to the maximum mean velocity (U_{max}), the suction intensity (Γ) was determined as the ratio of the transpiration velocity (V) to the mean bulk velocity (U) and the maximum mean velocity (U_{max}) is considered as 0.296 m/s.

Following the approach outlined by Ferro [6], the mean velocity profiles were scaled in outer coordinates using the maximum mean velocity. This method was adopted in the present study to facilitate the calculation of turbulence intensity.

Table 4 provides a concise overview of the benchmark test results obtained at both points, conducted under a Reynolds number of 1000. Additionally, Tables 5 and 6 present the filtration test data for points A and B, respectively.

Table.4 Summary of the results for benchmark case at both points. U_m is mean longitudinal velocity, SD is standard deviation, I_T is turbulence intensity, and Γ is suction intensity.

Test Name	**Re [-]**	**U_m [m/s]**	**SD [m/s]**	**I_T [-]**	**Γ [x10-4] [-]**
BN-A	1000	0.296	0.0181	0.061	-
BN-B	1000	0.266	0.0316	0.107	-

Table.5 Summary of the results for filtration case at point A. U_m is mean longitudinal velocity, SD is standard deviation, I_T is turbulence intensity, V_m is mean vertical velocity, and Γ is suction intensity.

Test Name	**Re [-]**	**U_m [m/s]**	**SD [m/s]**	**I_T [-]**	**V_m[x10^{-6}] [m/s]**	**Γ [x10^{-4}] [-]**
F-A-1	1000	0.28602	0.0143	0.0483	0.8621	0.0301
F-A-2	1000	0.28552	0.0141	0.0476	1.552	0.0544
F-A-3	1000	0.284	0.0140	0.0473	2.414	0.0850
F-A-4	1000	0.28071	0.0143	0.0483	3.276	0.1167
F-A-5	1000	0.27333	0.0139	0.0469	3.966	0.1451
F-A-6	1000	0.272	0.0139	0.0469	5	0.1838

Table.6 Summary of the results for filtration case at point B. U_m is mean longitudinal velocity, SD is standard deviation, I_T is turbulence intensity, V_m is mean vertical velocity, and Γ is suction intensity.

Test Name	Re [-]	U_m [m/s]	SD [m/s]	I_T [-]	V_m[x10^{-6}] [m/s]	Γ [x10^{-4}] [-]
F-B-1	1000	0.25356	0.0224	0.0757	0.8621	0.0340
F-B-2	1000	0.25518	0.0227	0.0767	1.552	0.0608
F-B-3	1000	0.25504	0.0223	0.0753	2.414	0.0947
F-B-4	1000	0.25329	0.0219	0.0740	3.276	0.1293
F-B-5	1000	0.24433	0.0220	0.0743	3.966	0.1623
F-B-6	1000	0.24905	0.0224	0.0757	5	0.2008

Based on the preceding measurements and calculations, as presented in the accompanying tables and Figure 16, the relationship between turbulence intensity and suction rate at a Reynolds number of 1000 for points A and B in both benchmark and filtration tests reveals the following:

i) A noticeable decrease in the standard deviation and, consequently, turbulent intensity at both points compared to the benchmark case. This reduction is more pronounced at point B than at point A.

ii) A lower suction rate at point A, which is located at the center of the test section, compared to point B.

iii) A relatively constant turbulence intensity across different suction rates. The slope of the curves representing the relationship between turbulence intensity and suction rate gradually decreases after the benchmark case and the initiation of the suction test, eventually tending towards a flat line with minimal deviations.

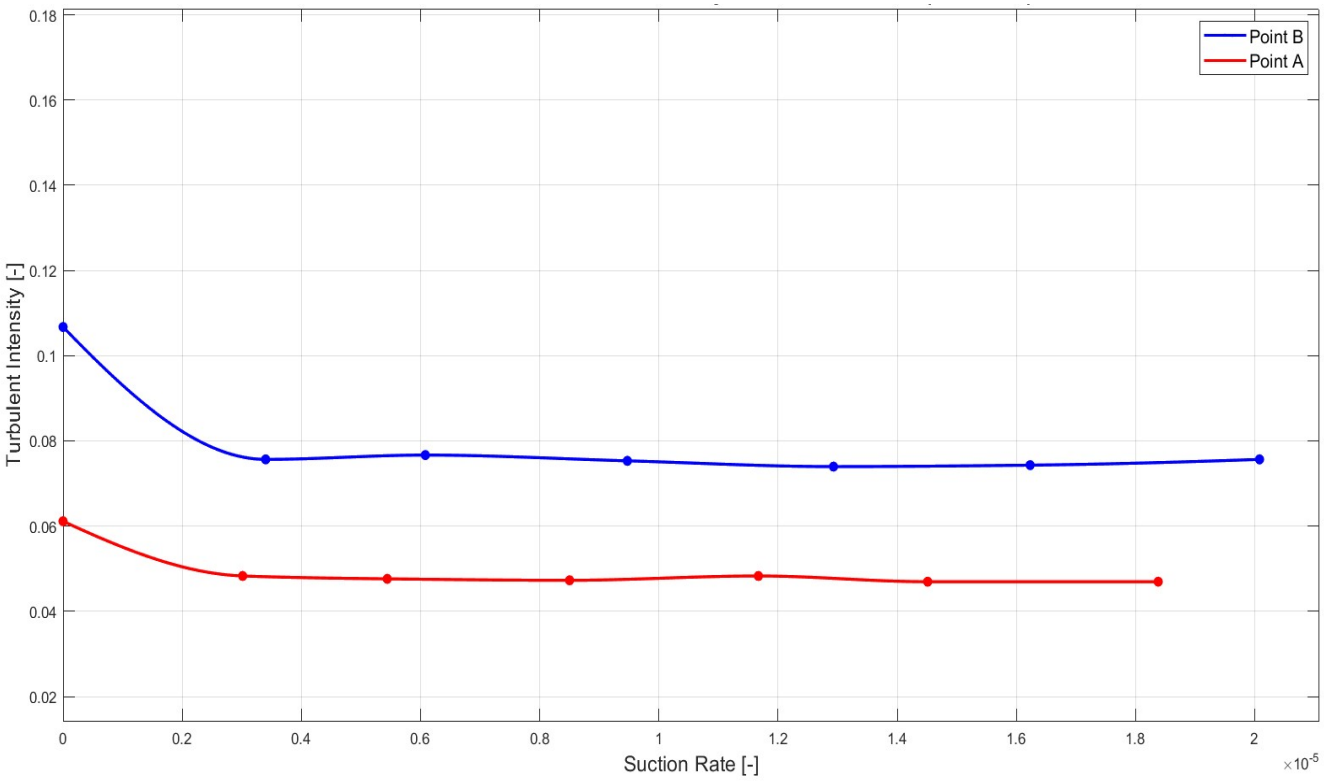

Fig.16 Suction rate Vs. turbulence intensity at both points A and B for benchmark and filtration tests.

4.2 Spectral Analysis

The Power Spectral Density (PSD) of a time series provides a frequency-domain interpretation, revealing how the signal's power is distributed across different frequencies. Prominent peaks in the PSD indicate periodic components at specific frequencies with significant amplitudes. For turbulent velocity time series, the PSD is commonly referred to as the Turbulence 1-D spectrum. Each PSD estimated represents the contribution of an eddy of frequency (f) to the total energy (variance) of the signal.

To ensure reliable spectral analysis, it's essential to compute smooth spectra with minimal noise. Applying the Fourier Transform, which transforms a time-domain signal into its frequency-domain representation, directly to the entire time series often yields noisy spectra. Welch's method offers a more robust approach. It involves segmenting the time series into windows, compute the spectra

for each of them and then take an average of PSD over different windows for each resolved frequency, to have a more robust PSD estimation. In MATLAB, the pwelch function facilitates PSD estimation using the syntax [S, f] = pwelch (y, window, overlap, nFFT, f_s). Here, y is the time series, window specifies the window size, overlap determines the overlap between windows (typically 50% to 12.5% of the window length), nFFT is the number of elements over which the algorithm works (usually the same as the window length), and f_s is the sampling frequency.

To effectively identify dominant eddy frequencies through spectral analysis, plotting premultiplied spectra is advantageous. Multiplying the PSD by the frequency aids in visualizing the contribution of each frequency to the signal's variance. This approach is particularly beneficial in semi-log coordinates, where differences are compressed, making it challenging to discern peaks.

Figure 17 and Figure 18 reveal the following observations:

i) **Premultiplied Power Spectral Density (PSD):** In comparison to the benchmark case, the peaks in the premultiplied power spectral density for both points diminished, suggesting a drop in the energy attributed to the dominant frequencies.

ii) **Length of Near-Wall Streaks in Longitudinal Direction:** Based on the Taylor hypothesis of frozen turbulence, which allows for the conversion from frequency (f) to wavenumber (k) in power spectral analysis, near-wall streaks in wall turbulence can be characterized. These streaks are generated by longitudinal vortices. To calculate the near-wall streak lengths, The friction velocity (u*) was determined from Bert's study [13] to be 0.0146 m/s and the relationships $k = 2\pi f/\bar{u}$ and $1/k = \lambda$ were employed, where f is the dominant eddy frequency (determined using Polyfit syntax in MATLAB to fit curves to premultiplied PSDs), $\bar{u}$ is the local time-averaged velocity, k is the wavenumber, λ is the average near-wall streak length, and ν is kinematic viscosity of water. By defining the normalized parameter λ^+ as $(\lambda * u^*)/\nu$, the values of λ^+ for the benchmark case were calculated to be approximately 1000 at point A and 1200 at point B. For the suction cases, λ^+ values were found to be around 1900 at point A and 2500 at point B.

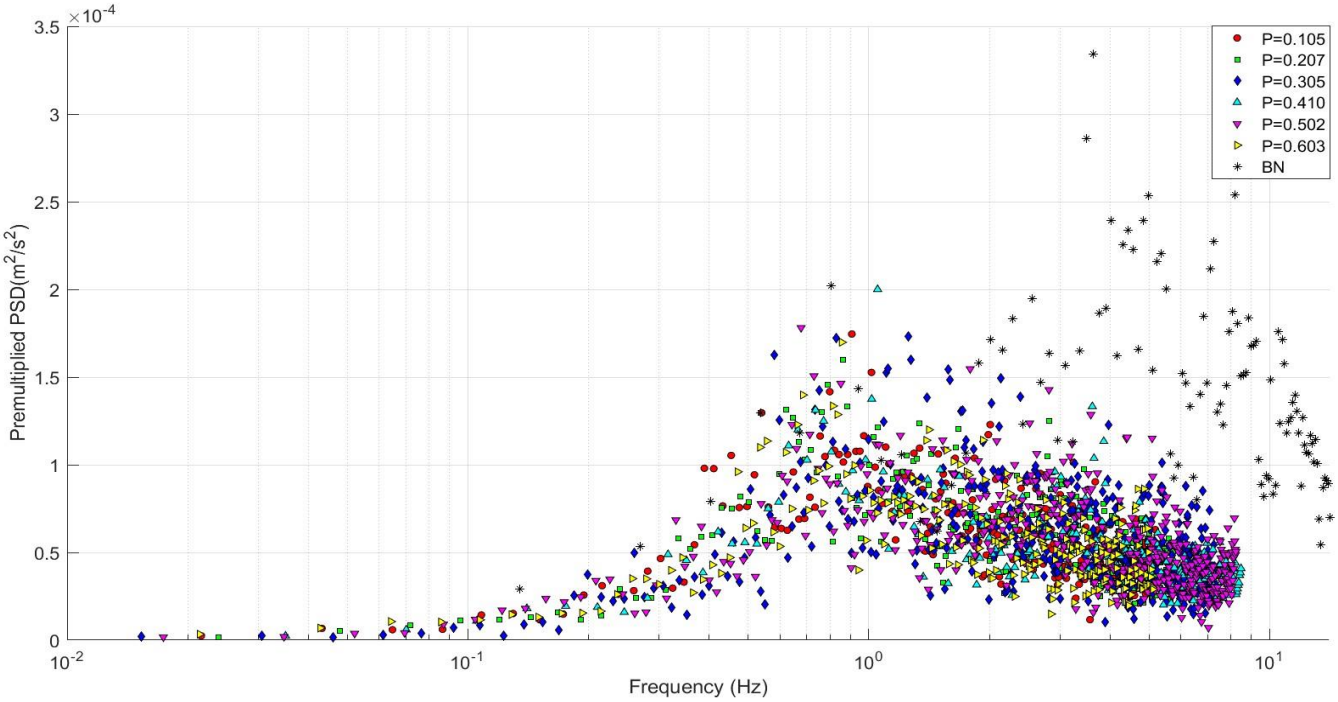

Fig.17 Premultiplied power spectral density Vs. frequency at point A (at center) for benchmark and filtration tests.

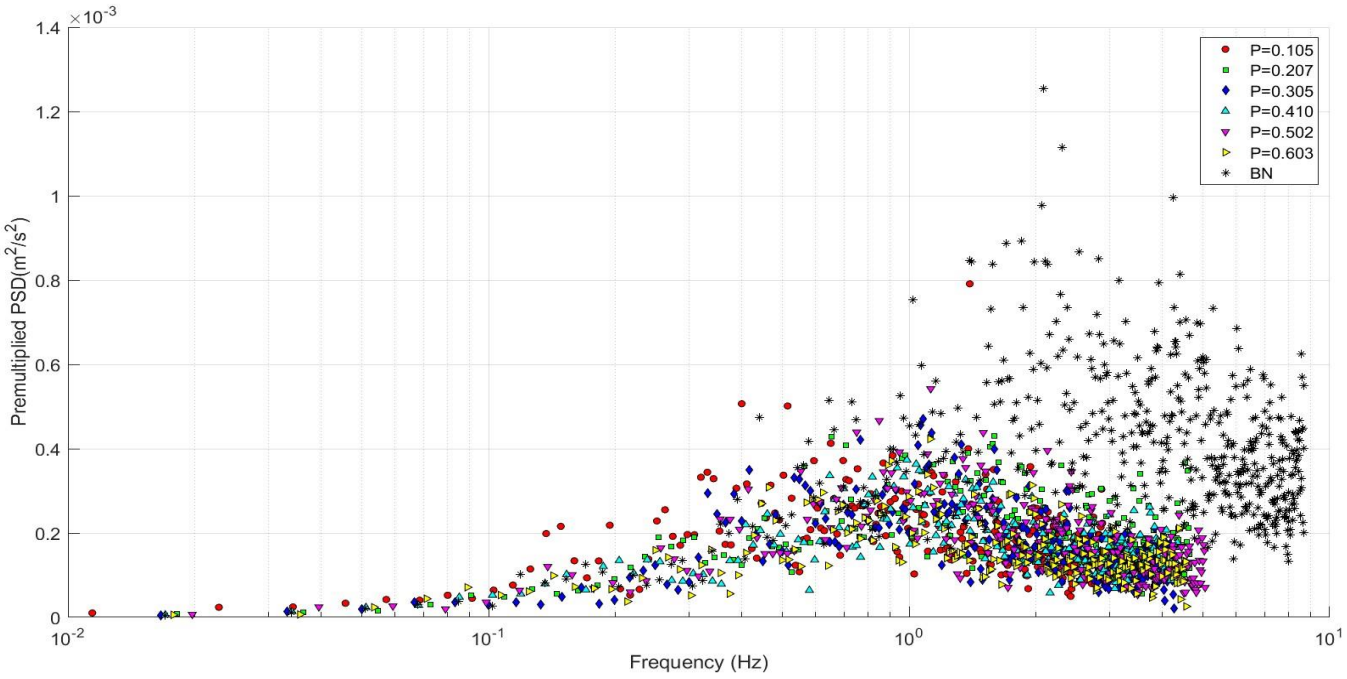

Fig.18 Premultiplied power spectral density Vs. frequency at point B (2.5mm from bottom) for benchmark and filtration tests.

Chapter 5

Conclusion

This section summarizes the key conclusions derived from the data presented in the previous chapter.

i) **Impact of Suction on Turbulence Damping**: The observed reduction in standard deviation and, consequently, turbulence intensity at both points A and B compared to the benchmark case demonstrates that suction effectively dampens turbulence. This effect is more pronounced closer to the wall (point B), where turbulence intensity is typically higher. This observation suggests that suction is particularly effective in stabilizing the flow near the wall region that is consistent with Bert findings [13].

ii) **Influence of Suction Rate on Turbulence Intensity**: The analysis of turbulence intensity versus suction rate reveals a surprising finding. The results indicate that turbulence intensity remains relatively constant across the range of suction rates induced by pressure variations at the tested Reynolds number of 1000. This suggests that, within the experimental parameters, turbulence intensity appears insensitive to variations in suction rate at both points A and B. Consequently, the observed damping of turbulence seems independent of the specific suction rate employed.

iii) **Effect of Suction on premultiplied PSD:** The premultiplied spectra at points A and B in the frequency domain demonstrate a significant reduction in velocity variance compared to the benchmark case. This indicates that suction effectively suppressed turbulent energy at these frequencies, resulting in an overall decrease in turbulence. This finding further supports the idea that suction stabilizes the flow, particularly near the wall. Moreover, the longer streaks observed near the wall in the suction cases suggest increased shear stress and elongated streak structures in this region. This expansion is more pronounced at point B, which is closer to the wall. Suction likely

contributed to the enlargement in streak length by damping turbulent fluctuations and stabilizing the flow near the wall.

The findings of this study demonstrate that suction effectively dampens turbulence within a rectangular channel, particularly near the wall region. This effect can be beneficial for enhancing membrane performance by reducing the detrimental effects of turbulent forces on the membrane, potentially leading to extended membrane lifespan.

It is important to note that turbulence can have both positive and negative effects on membranes. While excessive turbulence can lead to wear and tear, a certain level of turbulence can be beneficial in minimizing particle deposition on the membrane surface. Existing literature suggests an optimal range of Reynolds numbers exists where turbulence can be [21]. Striking a balance between minimizing clogging and preventing excessive wear is crucial for optimizing membrane performance and extending its lifespan.

While these findings offer valuable insights into the influence of suction on turbulence, further investigations are necessary to achieve a comprehensive understanding. Additional experiments encompassing a broader range of suction rates and Reynolds numbers are needed to establish the generalizability of these results. This comprehensive approach will allow for the identification of optimal suction parameters for achieving stable and efficient membrane operations that enhance both membrane longevity and resistance to clogging.

Bibliography

[1] UNESCO. (2024). *Report published on behalf of UN-Water*. United Nations Educational, Scientific and Cultural Organization. Retrieved from http://www.unwater.org

[2] Fiorillo, D., Kapelan, Z., Xenochristou, M., De Paola, F., & Giugni, M. (2021). *Assessing the Impact of Climate Change on Future Water Demand using Weather Data*. Water Resources Management, 35(5), 1449–1462. DOI: 10.1007/s11269-021-02789-4

[3] Ibrahim, M., Nawaz, M., Rout, P. R., Lim, J. W., Mainali, B., & Shahid, M. K. (2023). *Advances in Produced Water Treatment Technologies: An In-Depth Exploration with an Emphasis on Membrane-Based Systems and Future Perspectives*. Water, 15(16), 2980–2980. DOI: 10.3390/w15162980

[4] Bert, R., Manes, C., & Tiraferri, A. (2022). *New Facility for Membrane Fouling Investigations under Customizable Hydrodynamics: Validation and Preliminary Experiments with Pulsating Crossflow*. Membranes, 12(3), 334. DOI: 10.3390/membranes12030334

[5] Park, Y., Choi, Y., Choi, J., Ju, J., Kim, B., & Lee, S. (2020). *Effect of Vibration on Fouling Propensity of Hollow Fiber Membranes in Microfiltration and Membrane Distillation*. Desalination and Water Treatment, 192, 11–18. DOI: 10.5004/dwt.2020.25151

[6] Ferro, M. (2017). *Akademisk avhandling som med tillstånd av Kungliga Tekniska Högskolan i Stockholm framlägges till offentlig granskning för avläggande av teknologie doktorsexamen fredag den 24 November 2017 kl 10:15 i Kollegiesalen, Kungliga Tekniska Högskolan, Brinellvägen 8, Stockholm (TRITA-MEK 2017:13)*. Universitetsservice US AB. ISBN 978-91-7729-556-3.

[7] Yoshioka, S., & Alfredsson, P. H. (2006). *Control of Turbulent Boundary Layers by Uniform Wall Suction and Blowing*. In R. Govindarajan (Ed.), *IUTAM Symposium on Laminar-Turbulent Transition* (pp. 437-442). Springer. DOI: 10.1007/1-4020-4159-4_63

[8] Tennekes, H. (1964). *Similarity Laws for Turbulent Boundary Layers with Suction or Injection*. Aeronautical Engineering Department, Technological University, Delft.

[9] Black, T. J., & Sarnecki, A. J. (1958). *The Turbulent Boundary Layer with Suction or Injection*. Cambridge University Engineering Department.

[10] Dutton, R. A. (1958). *The Effects of Distributed Suction on the Development of Turbulent Boundary Layers*. Ministry of Aviation, Aeronautical Research Council, Engineering Laboratory, Cambridge.

[11] Kay, J. M. (1948). *Boundary-Layer Flow along a Flat Plate with Uniform Suction*. Cambridge University Engineering Laboratory.

[12] Khapko, T., Schlatter, P., Duguet, Y., & Henningson, D. S. (2016). *Turbulence Collapse in a Suction Boundary Layer*. Journal of Fluid Mechanics, 795, 356-379. DOI: 10.1017/jfm.2016.205

[13] Bert, R. (2021). *Hydrodynamic Techniques for Fouling Control in Membrane Systems* (Doctoral dissertation, Politecnico di Torino). Politecnico di Torino Institutional Repository. Retrieved from https://iris.polito.it/retrieve/07534d58-1822-4485-b89f-ca1c8f61bf8f/PhD_Thesis___Roberto_Bert___Hydrodynamic_Techniques_for_Fouling_Control_in_Membrane_Systems.pdf

[14] Bobke, A., Örlü, R., & Schlatter, P. (2016). *Simulations of Turbulent Asymptotic Suction Boundary Layers*. Springer Proceedings in Physics, 165, 31-47. DOI: 10.1007/978-3-319-29130-7_31

[15] Schildknecht, M., Miller, J. A., & Meier, G. E. A. (1978). *The Influence of Suction on the Structure of Turbulence in Fully Developed Pipe Flow*. Journal of Fluid Mechanics, 88(3), 501-528. DOI: 10.1017/S0022112078002264

[16] Antonia, R. A., Zhu, Y., & Sokolov, M. (1995). *Effect of Concentrated Wall Suction on a Turbulent Boundary Layer*. Physics of Fluids, 7, 2465. DOI: 10.1063/1.868690

[17] Kametani, Y., & Fukagata, K. (2011). *Direct Numerical Simulation of Spatially Developing Turbulent Boundary Layers with Uniform Blowing or Suction*. Journal of Fluid Mechanics, 681, 154-172. DOI: 10.1017/jfm.2011.219

[18] Zhang, Z. (2010). *LDA Application Methods: Laser Doppler Anemometry for Fluid Dynamics*. Springer. DOI: 10.1007/978-3-642-13514-9

[19] Liu, L., Chen, Z., Wu, W., Su, L., & Zhu, Y. (2023). *Numerical Study of Vortex Structures in a Centrifugal Pump Impeller with Tip Leakage Vortex Cavitation*. International Journal of Heat and Fluid Flow, 104, 109208. DOI: 10.1016/j.ijheatfluidflow.2023.109208

[20] Çengel, Y. A., & Cimbala, J. M. (2018). *Fluid Mechanics: Fundamentals and Applications* (5th ed.). McGraw-Hill Education.

[21] Duguet, Y. (2015). *Pipe Flow Clogged with Turbulence*. Journal of Fluid Mechanics, 776, 1–4. DOI: 10.1017/jfm.2015.285